The Astrophysical Journal, 790:114 (7pp), 2014 August 1 doi:10.1088/0004-637X/790/2/114

TRAJECTORY ANALYSIS FOR THE NUCLEUS AND DUST OF COMET C/2013 A1 (SIDING SPRING)

Davide Farnocchia[1], Steven R. Chesley[1], Paul W. Chodas[1], Pasquale Tricarico[2],
Michael S. P. Kelley[3], and Tony L. Farnham[3]
[1] Jet Propulsion Laboratory, California Institute of Technology,
Pasadena, CA 91109, USA; Davide.Farnocchia@jpl.nasa.gov
[2] Planetary Science Institute, Tucson, AZ 85719, USA
[3] Department of Astronomy, University of Maryland, College Park, MD 20742, USA
Received 2014 April 17; accepted 2014 June 13; published 2014 July 10

ABSTRACT

Comet C/2013 A1 (Siding Spring) will experience a high velocity encounter with Mars on 2014 October 19 at a distance of 135,000 km ± 5000 km from the planet center. We present a comprehensive analysis of the trajectory of both the comet nucleus and the dust tail. The nucleus of C/2013 A1 cannot impact on Mars even in the case of unexpectedly large nongravitational perturbations. Furthermore, we compute the required ejection velocities for the dust grains of the tail to reach Mars as a function of particle radius and density and heliocentric distance of the ejection. A comparison between our results and the most current modeling of the ejection velocities suggests that impacts are possible only for millimeter to centimeter size particles released more than 13 AU from the Sun. However, this level of cometary activity that far from the Sun is considered extremely unlikely. The arrival time of these particles spans a 20-minute time interval centered at 2014 October 19 at 20:09 TDB, i.e., around the time that Mars crosses the orbital plane of C/2013 A1. Ejection velocities larger than currently estimated by a factor >2 would allow impacts for smaller particles ejected as close as 3 AU from the Sun. These particles would reach Mars from 19:13 TDB to 20:40 TDB.

Key words: celestial mechanics – comets: individual (C/2013 A1) – methods: analytical – radiation: dynamics

1. INTRODUCTION

Comet C/2013 A1 (Siding Spring) was discovered on 2013 January at the Siding Spring observatory (McNaught et al. 2013). Shortly after discovery it was clear that C/2013 A1 was headed for a close encounter with Mars on 2014 October 19. C/2013 A1 is on a near parabolic retrograde orbit and will have a high relative velocity with respect to Mars of about 56 km s^{-1} during the close approach.

If the comet has no significant nongravitational perturbations, the trajectory of the nucleus consistent with the present set of astrometric observations rules out an impact on Mars. However, comet orbits are generally difficult to predict. As the comet gets closer to the Sun cometary activity can result in significant nongravitational perturbations (Marsden et al. 1973) that in turn can lead to significant deviations from the purely gravitational ("ballistic") trajectory. In the case of C/2013 A1, cometary activity was already visible in the discovery observations, when the comet was at more than 7 AU from the Sun (T. L. Farnham et al. 2014, in preparation; Ye & Hui 2014).

Besides the effect of nongravitational perturbations, dust grains in the tail of the comet could reach Mars and possibly damage spacecrafts orbiting Mars, i.e., NASA's Mars Reconnaissance Orbiter, NASA's Mars Odyssey, ESA's Mars Express, NASA's MAVEN, and ISRO's MOM. Vaubaillon et al. (2014) and Moorhead et al. (2014) show that dust grains can reach Mars if they are ejected from the nucleus with a sufficiently high velocity.

The modeling of the ejection velocities is in continuous evolution. As the comet gets closer to the inner solar system we have additional observations that provide constraints to the ejection velocities of dust grains. In particular, by making use of observations from *HST*/WFC3, *Swift*/UVOT, and *WISE*, T. L. Farnham et al. (2014, in preparation) and Tricarico et al. (2014) find ejection velocities lower than those derived by Vaubaillon et al. (2014) and Moorhead et al. (2014), thus significantly reducing the hazard due to dust grains in the comet tail.

In this paper, we study the trajectory of C/2013 A1's nucleus, including the contribution of nongravitational perturbations. We also present an analysis of the required ejection velocities for the dust grains to reach Mars. This analysis can be used as a reference as the understanding and the modeling of the dust grain ejection velocities evolve.

2. BALLISTIC TRAJECTORY

We examined all ground-based optical astrometry (right ascension and declination angular pairs) reported to the Minor Planet Center[4] as of 2014 March 15. To remove biased contributions from individual observatories we conservatively excluded from the orbital fit batches of more than four observations in the same night with mean residuals larger than 0.″5, and batches of three or four observations showing mean residuals larger than 1″. We also adopted the outlier rejection scheme of Carpino et al. (2003) with $\chi_{\rm rej} = 2$. To the remaining 597 optical observations we applied the standard one arcsecond data-weights used for comet astrometry. Figure 1 shows the residuals of C/2013 A1's observations against our new orbit solution (JPL solution 46).

Our force model included solar and planetary perturbations based on JPL's planetary ephemerides DE431 (Folkner et al. 2014), the gravitational attraction due to the 16 most massive bodies in the main asteroid belt, and the Sun relativistic term. No significant nongravitational forces were evident in the astrometric data and so the corresponding JPL orbit solution is ballistic, identified as number 46. Table 1 contains the orbital elements of the computed solution.

Table 2 provides information on the close encounter between C/2013 A1 and Mars. C/2013 A1 passes through the

[4] http://www.minorplanetcenter.net/

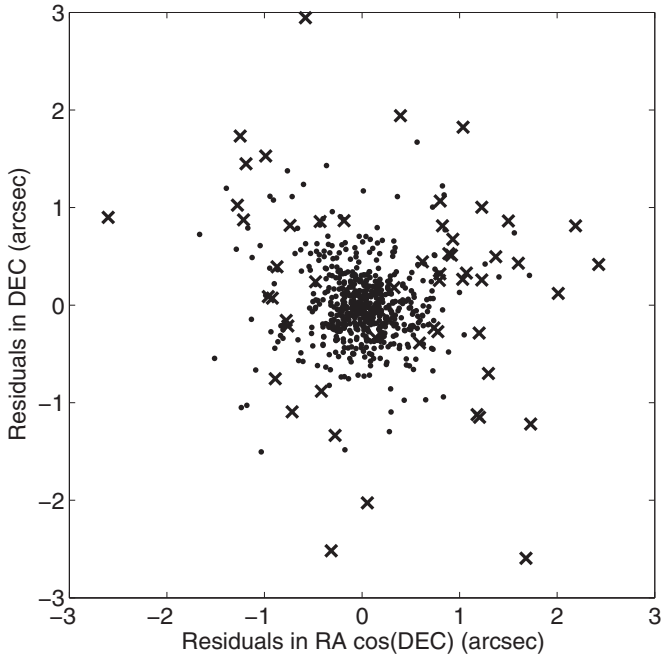

Figure 1. Scatter plot of the astrometric residuals in right ascension and declination with respect to JPL solution 46. Crosses correspond to rejected observations, while dots correspond to the observations included in the fit.

Table 1
J2000 Heliocentric Ecliptic Orbital Parameters of JPL Orbit Solution 46

Epoch TDB	2013 Aug 1.0
Eccentricity	1.0006045(61)
Perihelion distance (AU)	1.3990370(73)
Time of perihelion passage (TDB)	2014 Oct 25.3868(14)
Longitude of node (°)	300.974337(84)
Argument of perihelion (°)	2.43550(33)
Inclination (°)	129.026659(32)

Notes. Numbers in parentheses indicate the 1σ formal uncertainties of the corresponding (last two) digits in the parameter value.

Table 2
Close Approach Data for JPL Orbit Solution 46

Close approach epoch ($\pm 3\sigma$)	2014 Oct 19 18:30 TDB ±3 minutes
Close approach distance ($\pm 3\sigma$)	134,680 km ± 4520 km
Asymptotic relative velocity (v_∞)	55.96 km s^{-1}
MOID	27,414 km
Node crossing distance	27,563 km
Mars's arrival at line of nodes	2014 Oct 19 20:09 (TDB)
C/2013 A1's arrival at line of nodes	2014 Oct 19 17:21 (TDB)
Mars's arrival at MOID	2014 Oct 19 20:11 (TDB)
C/2013 A1's arrival at MOID	2014 Oct 19 17:20 (TDB)

orbital plane of Mars 69 minutes before the close approach epoch, while Mars passes through the orbital plane of C/2013 A1 at 20:09 TDB. The Minimum Orbit Intersection Distance (MOID) is the minimum distance between the orbit of the comet and the orbit of Mars (MOID; Gronchi et al. 2007). The MOID points on the two orbits are not on the line of nodes. Mars arrives at the minimum distance point at 20:11 TDB, while C/2013 A1 arrives at the minimum distance point 70 minutes before the close approach, which means that the comet is 171 minutes early for the minimum distance encounter.

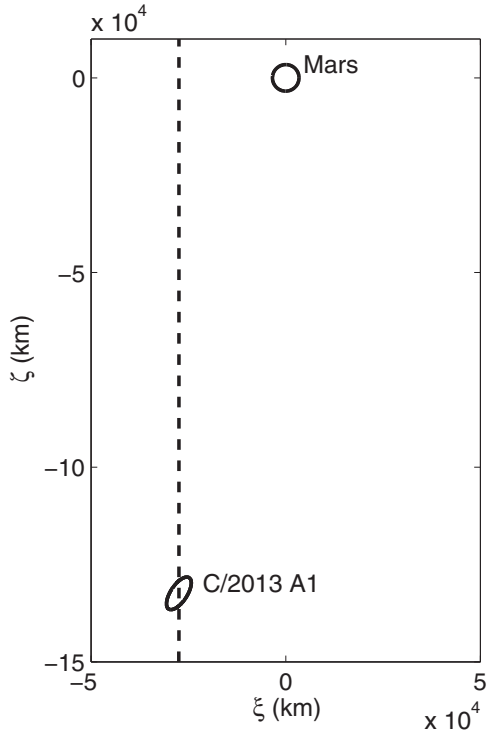

Figure 2. Projection of the 3σ uncertainty of JPL solution 46 on the 2014 October b-plane. The nominal prediction for the b-plane coordinates is $(\xi, \zeta) = (-27{,}445, -132{,}407)$ km. The dashed line represents the projection of the orbit of C/2013 A1 on the b-plane. The minimum distance between the orbits of Mars and C/2013 A1 is ∼27,400 km.

A standard tool to analyze planetary encounters is the b-plane (Kizner 1961; Valsecchi et al. 2003), defined as the plane passing through the center of mass of the planet and normal to the inbound hyperbolic approach asymptote. The coordinates on the b-plane described in Valsecchi et al. (2003) are oriented such that the projected heliocentric velocity of the planet is along $-\zeta$. Therefore, ζ varies with the time of arrival, i.e., a positive ζ means that the comet arrives late at the encounter while a negative ζ means that the comet arrives early. On the other hand, ξ is related to the MOID. The b-plane is used on a daily basis for asteroid close approaches to the Earth and computing the corresponding impact probabilities (Milani et al. 2005).

Figure 2 shows the projection of the 3σ uncertainty ellipsoid of JPL solution 46 on the b-plane. The projection of the velocity of Mars on this plane is oriented as $-\zeta$, while the Mars-to-Sun vector projection is on the left side, at a counterclockwise angle of 186° with respect to the ξ axis. The negative ζ coordinate of the center of the ellipse corresponds to the 171 minute time shift between Mars and C/2013 A1.

3. NONGRAVITATIONAL PERTURBATIONS

Comet trajectories can be significantly affected by nongravitational perturbations due to cometary outgassing. We use the Marsden et al. (1973) comet nongravitational model:

$$\mathbf{a}_{NG} = g(r)(A_1\hat{\mathbf{r}} + A_2\hat{\mathbf{t}} + A_3\hat{\mathbf{n}}),$$
$$g(r) = \alpha\left(\frac{\mathbf{r}}{\mathbf{r_0}}\right)^{-\mathbf{m}}\left[\mathbf{1} + \left(\frac{\mathbf{r}}{\mathbf{r_0}}\right)^{\mathbf{n}}\right]^{-\mathbf{k}} \quad (1)$$

where r is the heliocentric distance, $m = 2.15$, $n = 5.093$, $k = 4.6142$, $r_0 = 2.808$ AU, and α is such that $g(1\text{ AU}) = 1$.

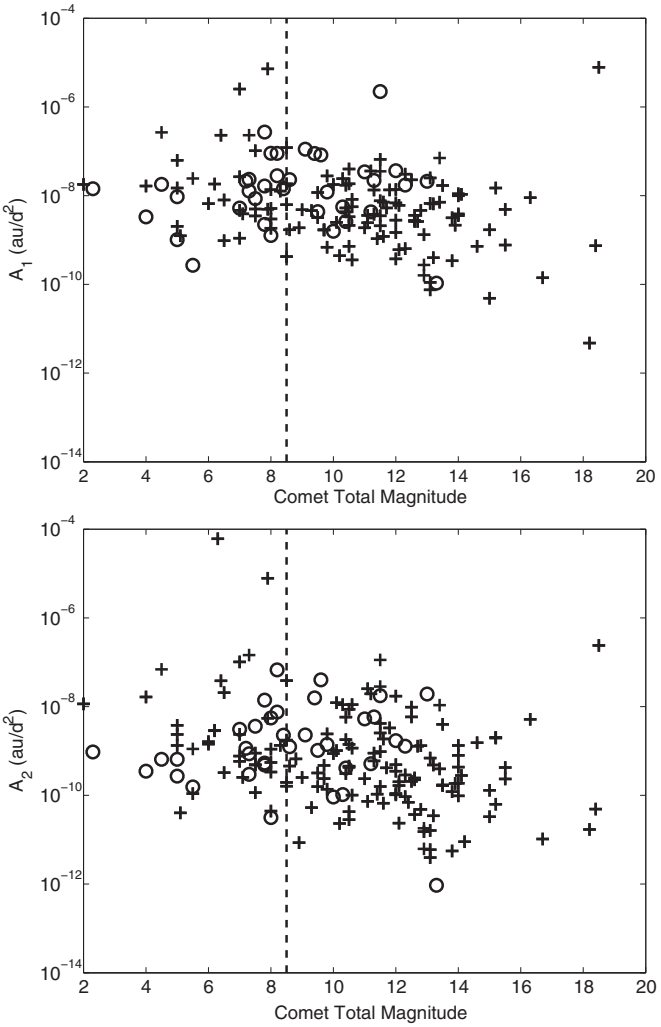

Figure 3. Estimated nongravitational parameters A_1 and A_2 for the comets in the catalog. A_2 is reported in absolute value. Circles correspond to comets with a period larger than 60 years or an eccentricity larger than 0.9. Crosses are for all other comets. The dashed line corresponds to the total magnitude of C/2013 A1.

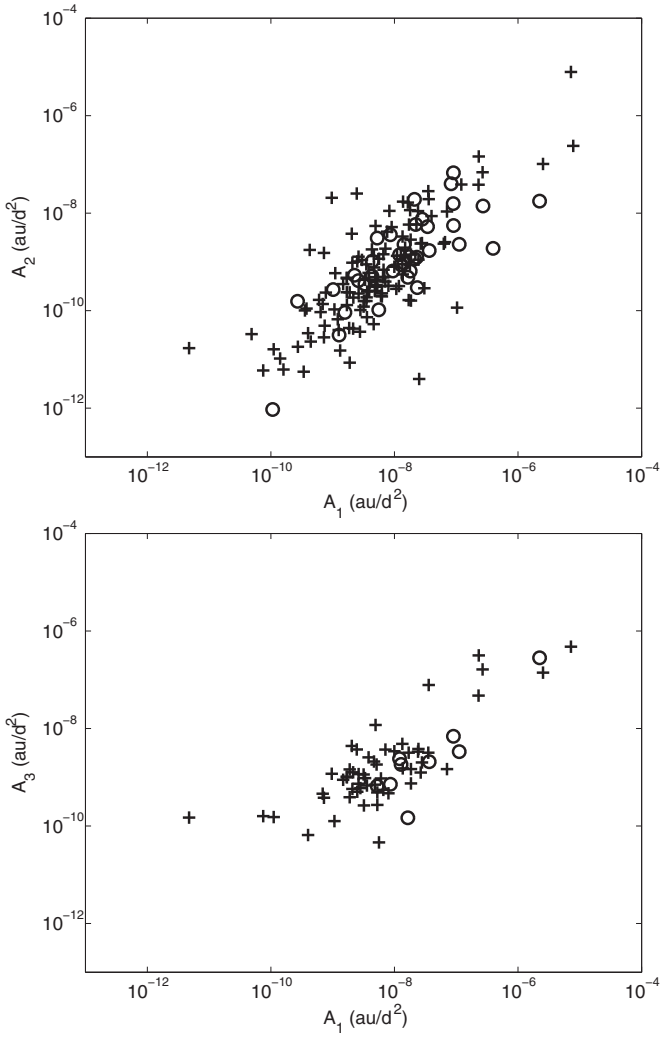

Figure 4. Scatter plots for nongravitational parameters A_1, A_2, and A_3. A_2 and A_3 are reported in absolute value. Circles correspond to comets with a period larger than 60 years or an eccentricity larger than 0.9. Crosses are for all other comets.

Therefore, A_1, A_2, and A_3 are free parameters that give the nongravitational acceleration at 1 AU in the radial–transverse–normal reference frame defined by $\hat{\mathbf{r}}$, $\hat{\mathbf{t}}$, $\hat{\mathbf{n}}$.

The observational data set available for C/2013 A1 does not allow us to estimate the nongravitational parameters A_i. Still, nongravitational accelerations could cause statistically significant deviations at the close approach epoch. To deal with this problem, we analyzed the properties of known nongravitational parameters in the comet catalog. Figure 3 shows the known A_1 and A_2 in the catalog. A_3 values have an order of magnitude similar to that of A_2. Figure 4 contains scatter plots of nongravitational parameters showing the correlation between these parameters. For comets with an orbit similar to that of C/2013 A1, i.e., with large orbital period (>60 years) and high eccentricity (>0.9), values of A_1 are on average $\sim 10^{-8}$ AU day^{-2}, but they can be as large as $\sim 10^{-6}$. A_2 and A_3 are generally one order of magnitude smaller, i.e., on average they are $\sim 10^{-9}$ AU day^{-2} but can be as large as $\sim 10^{-7}$ AU day^{-2}. We can see that A_1 is generally one order of magnitude larger than A_2 and A_3, which makes sense since the radial component is usually the largest for nongravitational accelerations.

According to the properties of the comet population we considered three different scenarios as described in Table 3:

Table 3
A Priori Values and 3σ Uncertainties of Nongravitational Parameters for the Three Scenarios

Scenario	A_1 (AU day^{-2})	A_2 (AU day^{-2})	A_3 (AU day^{-2})
Ballistic	0 ± 0	0 ± 0	0 ± 0
Reference	$(1 \pm 1) \times 10^{-8}$	$(0 \pm 2) \times 10^{-9}$	$(0 \pm 2) \times 10^{-9}$
Wide	$(1 \pm 1) \times 10^{-6}$	$(0 \pm 2) \times 10^{-7}$	$(0 \pm 2) \times 10^{-7}$

the ballistic scenario corresponds to JPL solution 46; the "reference" scenario uses typical values of the nongravitational parameters; the "wide" scenario assumes extreme values of the nongravitational parameters. We selected the A_1 uncertainty so that its range would span from 0 AU day^{-2} to twice the nominal value at 3σ. For A_2 and A_3 the nominal value is 0 AU day^{-2} since these components can be either positive or negative, while A_1 can only be positive.

Figure 5 shows the position difference among the three scenarios compared to the position uncertainty of the ballistic solution. The available observations put a strong constraint on the trajectory of C/2013 A1 for heliocentric distances between 3 AU and 8 AU from the Sun. Outside of this distance range we

Table 4
Close Approach Parameters and Uncertainties for the Three Scenarios

Scenario	ξ (km)	ζ (km)	3σ SMA (km)	TCA (TDB) $\pm$ 3σ
Ballistic	−27,445	−132,407	4789	2014 Oct 19 18:30 $\pm$ 3 minutes
Reference	−25,865	−131,671	5047	2014 Oct 19 18:30 $\pm$ 3 minutes
Wide	128,124	−58,610	174,882	2014 Oct 19 19:15 $\pm$ 45 minutes

Notes. The table shows the b-plane coordinates, the semimajor axis of the 3σ uncertainty projected on the b-plane, and the time of closest approach.

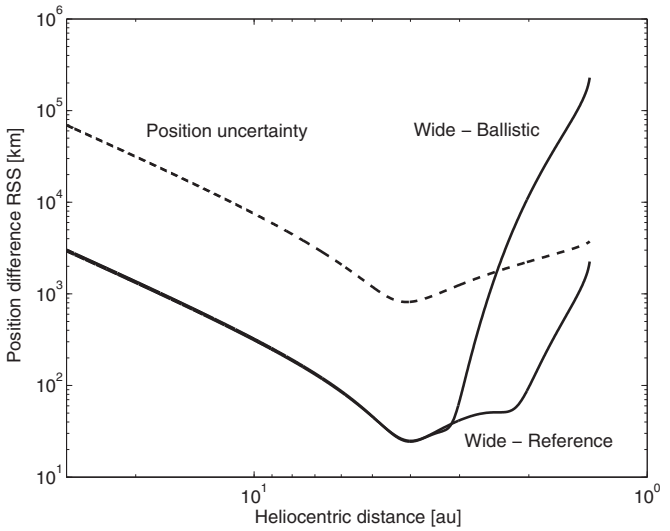

Figure 5. Magnitude of the position difference between the reference and ballistic solutions, and between the wide and ballistic solutions, as a function of heliocentric distance. The dashed line is the semimajor axis of the 1σ uncertainty ellipsoid of the ballistic solution.

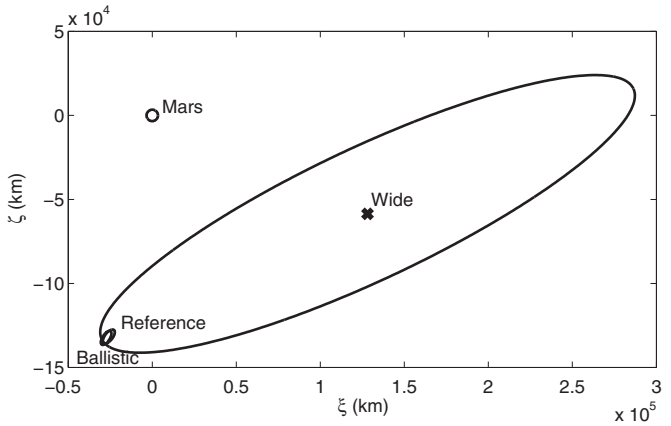

Figure 6. Projection on the b-plane of the 3σ position uncertainty of C/2013 A1 according to different scenarios for nongravitational perturbations. The ballistic and reference solutions are almost indistinguishable.

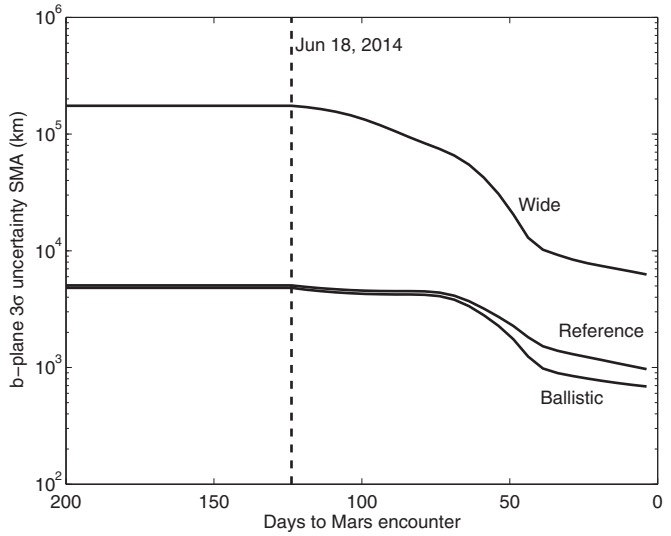

Figure 7. Expected evolution of the b-plane position uncertainty. The curves represent the semimajor axis of the projection on the b-plane of the 3σ uncertainty ellipse for the three scenarios. The vertical bar corresponds to 2014 June 18 when the solar elongation of C/2013 A1 becomes larger than 60°.

have no observations and therefore the uncertainty increases. Because of the fast decay of the $g(r)$ function in Equation (1) the contribution of nongravitational accelerations for heliocentric distances larger than 3 AU is well within the uncertainty and so the trajectory of C/2013 A1 in the past is not significantly affected. It is worth pointing out that the function $g(r)$ represents water sublimation while distant activity is not driven by water and therefore may be inaccurate at large distances. However, for such large distances the position uncertainty is large enough to make this possible discrepancy irrelevant. Finally, for smaller heliocentric distances, nongravitational perturbations become relevant and can affect the predictions for the Mars encounter, especially in the wide scenario.

For the three different scenarios, Table 4 gives the close approach information while Figure 6 shows the projection of the orbital uncertainties on the b-plane. The ballistic and reference solutions provide very similar predictions, from which we conclude that nongravitational perturbations will not significantly affect the orbit unless they are larger than expected. The wide solution, which has to be regarded as an extreme case, produces a significantly different nominal prediction and quite a large uncertainty. In all three scenarios, the nominal close approach distance is more than 130,000 km from Mars and therefore there is no chance of an impact between the nucleus of C/2013 A1 and Mars.

4. UNCERTAINTY EVOLUTION

The predictions and the uncertainty provided so far are based on the optical astrometry available as of 2014 March 15. At the time of submission of this paper (2014 April), comet C/2013 A1 was difficult to observe because of the low solar elongation. On 2014 June 18 the solar elongation becomes larger than 60° and we therefore expect observations to resume, which will help in further constraining the trajectory of C/2013 A1. To quantify the effect of future optical astrometry, we simulated geocentric optical observations, with two observations every five nights.

Figure 7 shows the evolution of the position uncertainty on the b-plane. The curves represent the semimajor axis of the projection of the 3σ uncertainty ellipsoid on the b-plane.

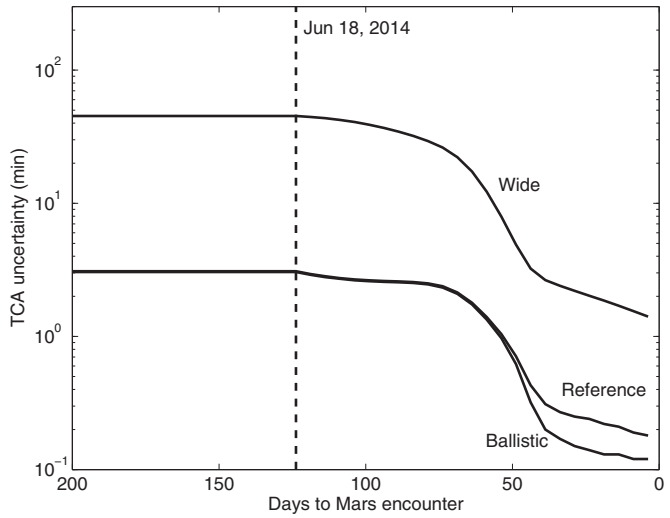

Figure 8. Expected evolution of the 3σ uncertainty of the closest approach epoch. The vertical bar corresponds to 2014 June 18 when the solar elongation of C/2013 A1 becomes larger than 60°.

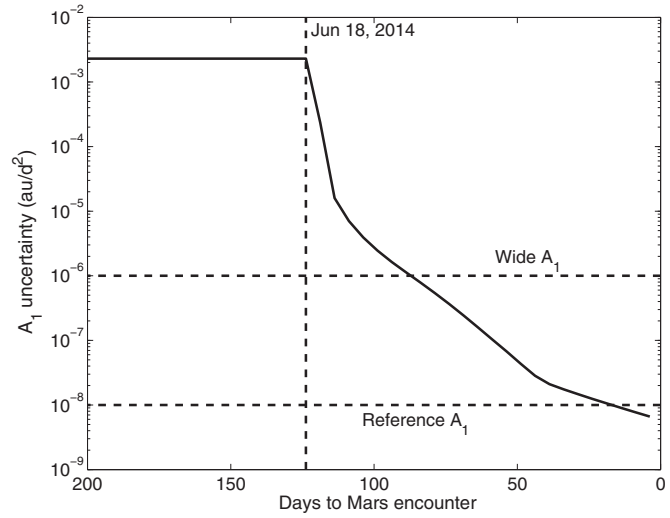

Figure 9. Expected evolution of the A_1 uncertainty (1σ). The horizontal dashed lines are for the nominal values of A_1 in the reference and wide scenarios. The vertical bar corresponds to 2014 June 18 when the solar elongation of C/2013 A1 becomes larger than 60°.

The ballistic and reference solution curves are close, with an uncertainty that goes from the current 5000 km to less than 1000 km when all the pre-encounter observations are accounted for. The wide solution has a much larger uncertainty that decreases to a minimum of about 6000 km.

Figure 8 shows the 3σ uncertainty evolution for the close approach epoch. The ballistic and reference scenarios have a current uncertainty of 3 minutes and this uncertainty decreases to less than 0.2 minutes right before the close approach. For the wide scenario the uncertainty goes from 45 minutes down to 1–2 minutes.

As already discussed in Section 3, the wide solution produces predictions significantly different from the ballistic and reference solutions. Thus, at some point observations will reveal whether or not the nongravitational perturbations are behaving as in the wide scenario. Figure 9 shows the uncertainty in A_1 when estimated from the orbital fit as a function of time. When this uncertainty becomes smaller than a given value of A_1, the observation data set reveals such A_1 value if it is real. By comparing

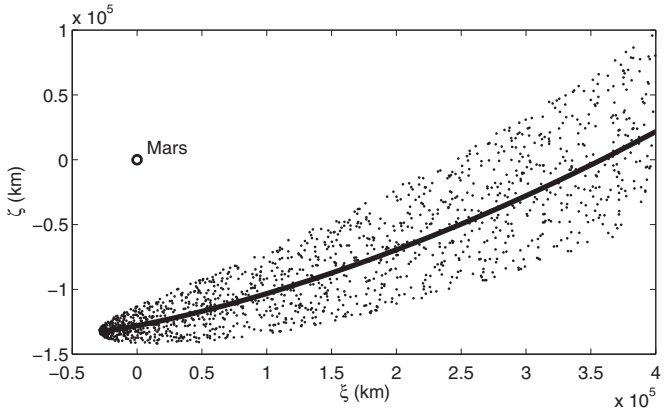

Figure 10. Projection on the b-plane of particles ejected with $\Delta v = 10$ m s^{-1} and for $\beta = 0.01$. The solid line represents the position of the particles with no Δv.

the uncertainty evolution to the nominal values of A_1 assumed for the different scenarios, we can see that large nongravitational accelerations to the level assumed in the wide scenario are detectable about 90 days before the close encounter. On the other hand, the reference solution becomes distinct from the ballistic solution only a couple of weeks before the encounter.

Some skilled observers are capable of gathering comet observations even for solar elongations smaller than 60°. Therefore, we also simulated observations using 40° as a lower threshold for the solar elongation, which makes it possible to collect new observations for C/2013 A1 starting on 2014 May 7. However, the improvement in the uncertainties discussed above is a factor of 1.3 or less and is therefore not relevant.

5. DUST TAIL

Though an impact of the nucleus of C/2013 A1 on Mars is ruled out, there is a chance that dust particles in the tail could reach Mars and some of the orbiting spacecrafts. Due to their small size, the motion of dust particles is strongly affected by solar radiation pressure. It is therefore convenient to use the β parameter (Burns et al. 1979), i.e., the non-dimensional number corresponding to the ratio between solar radiation pressure and solar gravity. In terms of physical properties, β is proportional to the area-to-mass ratio and inversely proportional to both the density and to the radius of the particle:

$$\beta = \frac{0.57\, Q}{a\rho} \tag{2}$$

where a is the particle radius in μm, ρ is the density in g/cm^3, and Q is the solar radiation pressure efficiency coefficient.

For each ejected particle, the location on the b-plane for the Mars encounter is determined by the β parameter, the heliocentric distance r at which the particle is ejected (or the ejection epoch), and the ejection velocity $\Delta\mathbf{v}$. Figure 10 shows the typical behavior using as an example $\beta = 0.01$ and $\Delta v = |\Delta\mathbf{v}| = 10$ m s^{-1}. For each given β, we have a curve on the b-plane corresponding to zero ejection velocity. This curve can be parameterized by the heliocentric distance at which the ejection takes place. Finally, the ejection velocity $\Delta\mathbf{v}$ yields dispersion around the curve: the larger the Δv the wider the dispersion.

The ejection velocity depends on the particle size and density, as well as the heliocentric distance at which the particle is ejected (Whipple 1951). Since cometary activity is very hard to predict,

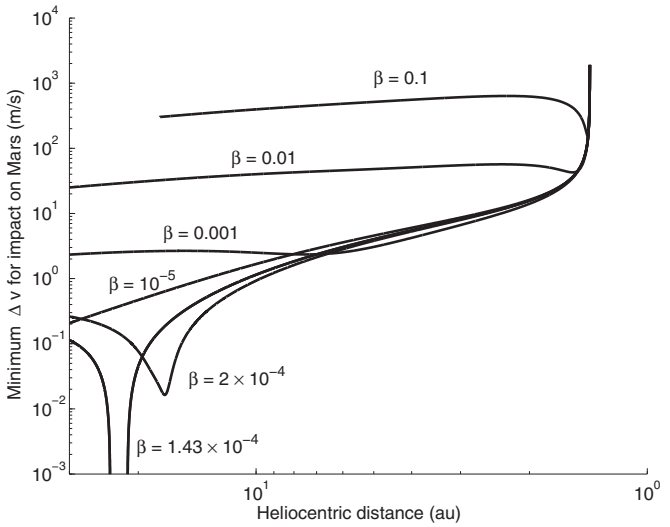

Figure 11. For different values of β, required Δv to reach Mars as a function of the heliocentric distance at which the ejection takes place.

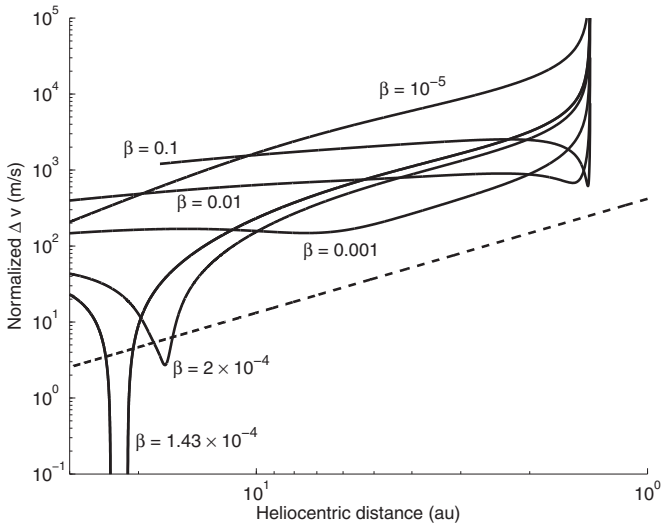

Figure 12. Required Δv to reach Mars multiplied by $(1/\beta)^{0.6}$. The dashed line corresponds to $\Delta v = 418\,\mathrm{m\,s^{-1}}\beta^{0.6}(1\,\mathrm{AU}/r)^{1.5}$. Impacts are possible only for particles ejected more than 16 AU from the Sun and with $\beta \sim 2 \times 10^{-4}$ or smaller.

modeling the ejection velocities is a complicated task and is subject to continuous updates as additional observations are available. Therefore, we decided to adopt a different approach: for given ejection distance r and β parameter, we computed the minimum Δv required to reach Mars. In mathematical terms we look for the tridimensional $\Delta\mathbf{v}$ that is a minimum point of $\Delta v^2 = |\Delta\mathbf{v}|^2$ under the constraint that the particle reaches Mars, i.e., $(\xi, \zeta)(r, \beta, \Delta\mathbf{v}) = (0, 0)$.

This problem is a typical example of finding the minima of a function subject to equality constraints. Thus, we can solve this problem by means of the Lagrange multipliers, i.e., the $\Delta\mathbf{v}$ we are looking for must satisfy the following system of equations:

$$\begin{cases} (\xi, \zeta)(r, \beta, \Delta\mathbf{v}) = (0, 0) \\ \dfrac{\partial |\Delta\mathbf{v}|^2}{\partial \Delta\mathbf{v}} = \lambda_1 \dfrac{\partial \xi}{\partial \Delta\mathbf{v}}(r, \beta, \Delta\mathbf{v}) + \lambda_2 \dfrac{\partial \zeta}{\partial \Delta\mathbf{v}}(r, \beta, \Delta\mathbf{v}) \end{cases}, \tag{3}$$

where λ_1 and λ_2 are free parameters. To solve this system, we first tested the linearity of (ξ, ζ) in $\Delta\mathbf{v}$ and then linearized system (3) around $\Delta\mathbf{v} = 0$, thus obtaining the following linear system:

$$\begin{cases} (\xi, \zeta)(r, \beta, \Delta\mathbf{v}) = (\xi, \zeta)(r, \beta, 0) + \dfrac{\partial(\xi, \zeta)}{\Delta\mathbf{v}}(r, \beta, 0)\Delta\mathbf{v} = (0, 0) \\ 2\Delta\mathbf{v} = \lambda_1 \dfrac{\partial \xi}{\partial \Delta\mathbf{v}}(r, \beta, 0) + \lambda_2 \dfrac{\partial \zeta}{\partial \Delta\mathbf{v}}(r, \beta, 0). \end{cases} \tag{4}$$

To compute the required $\Delta\mathbf{v}$, we followed these steps:

1. We uniformly sampled β in log scale with factor of 10 steps between 10^{-6} and 1;
2. We sampled r from 1.4 AU to 30 AU by using a 10 day step along the trajectory;
3. For each couple (r, β) we computed the b-plane coordinates (ξ, ζ) obtained without ejection velocity as well as a finite difference approximation of the (ξ, ζ) partials with respect to $\Delta\mathbf{v}$;
4. We solved system (4).

We scaled the resulting $\Delta\mathbf{v}$ to account for the size of Mars and the 3σ uncertainty of the particle projection on the b-plane. For this analysis, we used the ballistic solution as reference trajectory.

Figure 11 shows the required Δv needed to reach Mars as a function of the heliocentric distance at which the ejection takes place for different values of β. On the right side of the plot the required velocities are almost the same. This behavior makes sense as the closer we get to Mars the less time is available for solar radiation pressure to affect the trajectory. Therefore, the required ejection velocity is almost independent of the particle size and density. For $\beta = 1.43 \times 10^{-4}$, we can see that the required velocity goes to zero for heliocentric distances around 22.5 AU. As a matter of fact, the curve on the b-plane defined by this critical value of β passes through the center of Mars. Thus, if ejected at the right distance, i.e., 22.5 AU, the particle reaches Mars under the action of solar radiation pressure, with no ejection velocity at all. To properly describe the behavior around the critical value of β, we added 1.43×10^{-4} and 2×10^{-4} to the β sampling. It is also worth noticing that the $\beta = 0.1$ curve does not go all the way back to 30 AU because, for such a high β, solar radiation pressure is extremely strong and the particle does not even experience the close encounter with Mars if ejected too far in advance.

The results obtained so far can be used to assess the possibility that particles of a given size could reach Mars for a given ejection velocity model. For instance, the best fit for the ejection velocity according to T. L. Farnham et al. (2014, in preparation) is

$$\Delta v = 418\ \mathrm{m\ s^{-1}} \left(\frac{\beta}{1}\right)^{0.6} \left(\frac{1\ \mathrm{AU}}{r}\right)^{1.5}. \tag{5}$$

As shown in Figure 12, we can scale the required velocity to $\beta = 1$ and make a comparison to the velocity given by (5). We can see that, according to this ejection velocity model, impacts are possible only for particles with $\beta \sim 2 \times 10^{-4}$ or smaller ejected at more than ~16 AU from the Sun.

Figure 13 shows a comparison to the ejection velocity model considered by Tricarico et al. (2014):

$$\Delta v = 1.3\ \mathrm{m\ s^{-1}} \left(\frac{\beta}{5.7 \times 10^{-4}}\right)^{0.5} \left(\frac{5\ \mathrm{AU}}{r}\right)^{1}. \tag{6}$$

In this case, impacts are possible only for particles ejected more than 13 AU from the Sun and $\beta \sim 10^{-4}$. The figure also makes

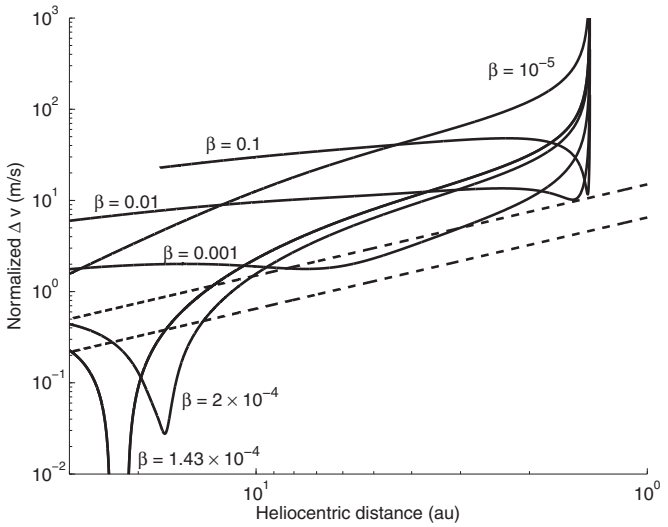

Figure 13. Required Δv to reach Mars multiplied by $(5.7 \times 10^{-4}/\beta)^{0.5}$. The lower dashed line corresponds to $\Delta v = 1.3\,\mathrm{m\,s^{-1}}(\beta/5.7 \times 10^{-4})^{0.5}(5\ \mathrm{AU}\ /\mathrm{r})^{1}$. In this case impacts are possible for particles ejected more than 13 AU from the Sun and $\beta \sim 2 \times 10^{-4}$ or smaller. The upper dashed line corresponds to $\Delta v = 3\,\mathrm{m\,s^{-1}}(\beta/5.7 \times 10^{-4})^{0.5}(5\ \mathrm{AU}\ /\mathrm{r})^{1}$. In this case impacts are possible also for $\beta = 0.001$ and particles ejected as close as ∼3 AU from the Sun.

the comparison for larger ejection velocities (also considered by Tricarico et al. 2014):

$$\Delta v = 3\ \mathrm{m\ s^{-1}} \left(\frac{\beta}{5.7 \times 10^{-4}}\right)^{0.5} \left(\frac{5\ \mathrm{AU}}{r}\right)^{1}. \qquad (7)$$

In this case, impacts are possible also for $\beta = 0.001$ and particles ejected as close as ∼3 AU from the Sun.

We conclude that impacts are possible only in one of these two unlikely cases:

1. millimeter to centimeter dust grains are ejected from the nucleus more than 13 AU from the Sun;
2. the ejection velocities are larger than current estimates by a factor >2.

In the first case, the particles can reach Mars during a 20 minute interval centered at the time that Mars crosses the orbit of C/2013 A1, i.e., 2014 October 19 at 20:09 (TDB). In the second case, the time interval is wider and goes from 19:13 TDB to 20:40 TDB. For an analysis of the probability distribution of the arrival times, see Tricarico et al. (2014) and Kelley et al. (2014).

6. CONCLUSIONS

To study the 2014 October 19 encounter with Mars, we analyzed the trajectory of comet C/2013 A1 (Siding Spring). The ballistic orbit has a closest approach with Mars at 135,000 km ±5000 km at 18:30 TDB.

Nongravitational perturbations are not yet detectable for C/2013 A1, so we assumed known nongravitational parameters for known comets in the catalog. In the case of typical nongravitational perturbations there are no relevant differences from the ballistic trajectory. On the other hand, unexpectedly large nongravitational accelerations would produce significant deviations that should become detectable in the observation data set by the end of 2014 July. However, even in the case of unexpectedly large nongravitational perturbations, the nucleus C/2013 A1 cannot reach Mars.

To analyze the risk posed by dust grains in the tail, we computed the required ejection velocities as a function of the heliocentric distance at which the particle is ejected and the particle's β parameter, i.e., the ratio between solar radiation pressure and solar gravity. By comparing our results to the most updated modeling of dust grain ejection velocities, impacts are possible only for β of the order of 10^{-4}, which, for a density of 1 g/cm^3, corresponds to millimeter to centimeter particles. However, the particles have to be ejected at more than 13 AU, which is generally considered unlikely. See Kelley et al. (2014) for a discussion of the maximum liftable grain size at these distances. The arrival times of these particles are in an interval of about 20 minutes around the time that Mars crosses the orbit of C/2013 A1, i.e., 2014 October 19 at 20:09 TDB. In the unlikely case that ejection velocities are larger than currently estimated by a factor >2, impacts are possible for particles with $\beta = 0.001$ that are ejected as close as ∼3 AU from the Sun. These impacts would take place from 43 minutes to 130 minutes after the nominal ballistic close approach of the nucleus.

As the comet gets closer to the inner solar system, new observations will be available and will allow better constraints on the dust grain ejection velocity profile. Our analysis can be used as a reference to quickly figure out what particles can reach Mars and the heliocentric distance at which they would have to have been ejected. These impacts would take place from 19:13 TDB to 20:40 TDB.

Part of this research was conducted at the Jet Propulsion Laboratory, California Institute of Technology, under a contract with the National Aeronautics and Space Administration.

REFERENCES

Burns, J. A., Lamy, P. L., & Soter, S. 1979, Icar, 40, 1
Carpino, M., Milani, A., & Chesley, S. R. 2003, Icar, 166, 248
Folkner, W. M., Williams, J. G., Boggs, D. H., Park, R. S., & Kuchynka, P. 2014, IPNPR, 196, 1
Gronchi, G. F., Tommei, G., & Milani, A. 2007, in IAU Symp. 236, Near Earth Objects, our Celestial Neighbors: Opportunity and Risk, ed. G. B. Valsecchi, D. Vokrouhlický, & A. Milani (Cambridge: Cambridge Univ. Press), 3
Kelley, M. S. P., Farnham, T. L., Bodewits, D., Tricarico, P., & Farnocchia, D. 2014, ApJ, submitted
Kizner, W. 1961, P&SS, 7, 125
Marsden, B. G., Sekanina, Z., & Yeomans, D. K. 1973, AJ, 78, 211
McNaught, R. H., Sato, H., & Williams, G. V. 2013, CBET, 3368, 1
Milani, A., Chesley, S. R., Sansaturio, M. E., Tommei, G., & Valsecchi, G. B. 2005, Icar, 173, 362
Moorhead, A. V., Wiegert, P. A., & Cooke, W. J. 2014, Icar, 231, 13
Tricarico, P., Samarasinha, N. H., Sykes, M. V., et al. 2014, ApJL, 787, L35
Valsecchi, G. B., Milani, A., Gronchi, G. F., & Chesley, S. R. 2003, A&A, 408, 1179
Vaubaillon, J., Maquet, L., & Soja, R. 2014, MNRAS, 439, 3294
Whipple, F. L. 1951, ApJ, 113, 464
Ye, Q.-Z., & Hui, M.-T. 2014, ApJ, 787, 115